Applied Physics Letters

186 K operation of terahertz quantum-cascade lasers based on a diagonal design

Cite as: Appl. Phys. Lett. **94**, 131105 (2009); https://doi.org/10.1063/1.3114418
Submitted: 09 February 2009 • Accepted: 14 March 2009 • Published Online: 01 April 2009

Sushil Kumar, Qing Hu and John L. Reno

186 K operation of terahertz quantum-cascade lasers based on a diagonal design

Sushil Kumar,[1,a)] Qing Hu,[1] and John L. Reno[2]
[1]*Department of Electrical Engineering and Computer Science and Research Laboratory of Electronics, Massachusetts Institute of Technology, Cambridge, Massachusetts 02139, USA*
[2]*Center of Integrated Nanotechnologies, Sandia National Laboratories, MS 1303, Albuquerque, New Mexico 87185-1303, USA*

(Received 9 February 2009; accepted 14 March 2009; published online 1 April 2009)

Resonant-phonon terahertz quantum-cascade lasers operating up to a heat-sink temperature of 186 K are demonstrated. This record temperature performance is achieved based on a diagonal design, with the objective to increase the upper-state lifetime and therefore the gain at elevated temperatures. The increased diagonality also lowers the operating current densities by limiting the flow of parasitic leakage current. Quantitatively, the diagonality is characterized by a radiative oscillator strength that is smaller by a factor of two from the least of any previously published designs. At the lasing frequency of 3.9 THz, 63 mW of peak optical power was measured at 5 K, and approximately 5 mW could still be detected at 180 K. © *2009 American Institute of Physics*. [DOI: 10.1063/1.3114418]

The past decade witnessed remarkable progress in the development of the midinfrared (IR) quantum-cascade lasers (QCLs),[1] and room-temperature continuous-wave operation is obtained over the $\lambda \sim 4-10$ μm spectrum. In contrast, invention of the terahertz ($\nu \sim 1-10$ THz, $\lambda \sim 30-300$ μm) QCLs has been more recent,[2] and there is still much to be desired in their performance, the foremost being operation at temperatures accessible by the present day thermoelectric coolers ($\gtrsim 240$ K) and ultimately at room temperature.

For an intersubband radiative transition from level $u \rightarrow l$, the peak gain $g \propto \Delta n_{ul} f_{ul} / \Delta\omega$, where Δn_{ul} is the population inversion, f_{ul} is the oscillator strength, and $\Delta\omega$ is the linewidth of the transition. For spontaneous emission, intersubband emitters have an inherently small radiative efficiency $\eta \approx \tau_{u\rightarrow l} / \tau_{\text{spont}}$ due to the fast electron-longitudinal-optical (e-LO) phonon scattering time in polar semiconductors. This, coupled with the fact that the spontaneous emission power output ($\propto \omega^2 f_{ul}$) is lower at terahertz frequencies, makes it difficult to distinguish terahertz intersubband emission from thermal blackbody radiation. Historically, prior to the realization of the first terahertz QCL, the design strategy had been to maximize f_{ul}, which tended to yield less ambiguous intersubband emission signals with narrow linewidths.[3–5] This strategy apparently contributed to the initial breakthrough of terahertz QCLs based on the chirped superlattice (CSL) structure.[2]

Despite this early success, however, the large f_{ul} corresponds to a vertical design in which the upper and lower states strongly overlap, resulting in a fast decrease in the upper-state lifetime with temperature in the form of $\tau_{u\rightarrow l} \approx \tau_{\text{LO}} \exp[(\hbar\omega_{\text{LO}} - \hbar\omega)/k_B T_e]$, where τ_{LO} is the raw LO-phonon scattering time when the upper-state electrons are sufficiently energetic to emit LO phonons and T_e is the electron temperature. In order to increase the operating temperature of terahertz QCLs, the key is to increase $\tau_{u\rightarrow l}$ at high temperatures. It is clear that $\tau_{u\rightarrow l}$ will have a sensitive temperature dependence in the exponential factor $\exp(\hbar\omega_{\text{LO}} - \hbar\omega)/k_B T_e$. This is a fundamental feature of terahertz QCLs since $\hbar\omega < \hbar\omega_{\text{LO}}$. Our recent work has demonstrated that $\tau_{u\rightarrow l}$ can be made longer by using a strong magnetic field to increase τ_{LO}, resulting in a maximum operating temperature ($T_{\max}$) of 225 K.[6] In this work, we explore another strategy to increase τ_{LO} (without using a magnetic field) by making the $u \rightarrow l$ transition diagonal. The advantages of a diagonal radiative transition are well known from the previous work in mid-IR QCLs. Even in the terahertz, the bound-to-continuum (BTC) transition based designs achieve a better performance due to increased diagonality.[7,8] In this work, we go a step further and make our design considerably more diagonal than the previous designs, which successfully led to a record temperature performance of 186 K. Furthermore, because of a greater spatial separation between the injector state and a lower parasitic state, the parasitic current density is lower than that of similar structures based on a vertical design.

Figure 1 shows the conduction band diagram of the design at two different bias conditions. The design is similar to a recently published three-well structure,[9] which had demonstrated the best $T_{\max}$ of 178 K for any terahertz QCL so far.[10] The key characteristics of this design are the resonant-phonon depopulation scheme[11] and a one-well injector region.[12] The (dimensionless) oscillator strength $f_{ul} \equiv (4\pi m^* \nu_{ul} z_{ul}^2)/\hbar$ (where z_{ul} is the radiative dipole matrix element, m^* is the effective mass, and ν_{ul} is the radiative frequency) can be considered a good measure for diagonality. A big difference in the present design is the value of $f_{ul} \approx 0.38$ ($z_{ul} \approx 37$ Å), which is less than half of the least of all previously published terahertz QCLs that operate above 2 THz. For comparison, $f_{ul} \approx 0.85$ in the design in Refs. 9, 10, and 13 and $f_{ul} \approx 0.77$ for a slightly modified version of the four-well design in Ref. 14 that yielded a $T_{\max}$ of 173 K.[15] Visually, Fig. 1(a) shows that the upper- and lower-state wave functions are localized in separate wells with little spatial overlap. Here we note that we use f_{ul} to compare diagonality of the resonant-phonon designs only; f_{ul} may not be an ideal parameter to compare the resonant-phonon designs

a)Electronic mail: sushil@mit.edu.

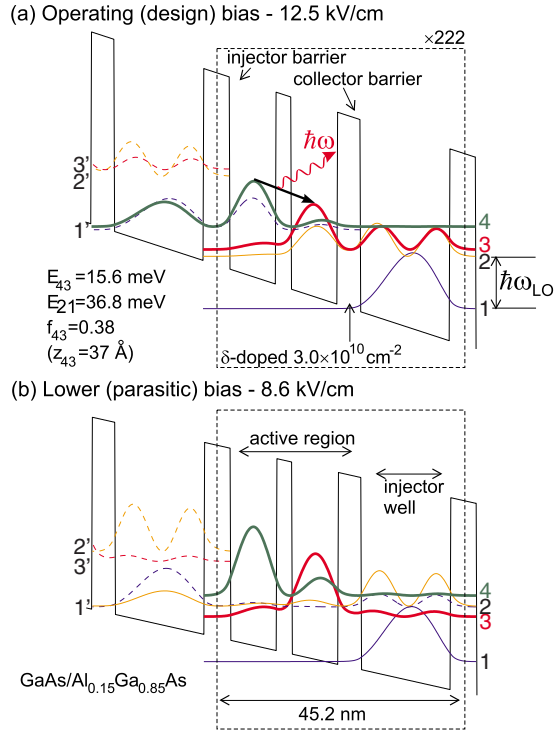

FIG. 1. (Color online) Conduction band diagram at (a) the operating bias and (b) a lower (parasitic) bias as characterized by the $1' \rightarrow 4$ and the $1' \rightarrow 2$ alignments, respectively. $1'$ is the injector level from the preceding module and the radiative transition is from $4 \rightarrow 3$ ($\nu \approx E_{43}/h \approx 3.8$ THz). Starting from the injector barrier, the layer thicknesses in nanometer are **4.8**/8.5/**2.8**/8.5/**4.2**/16.4, with the barriers indicated in bold fonts.

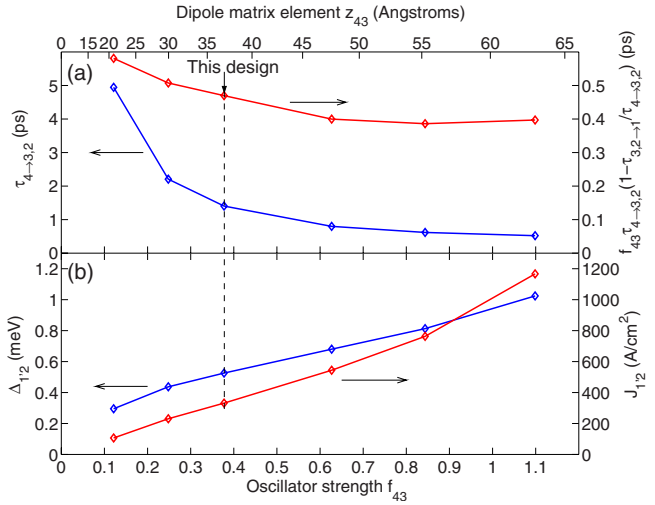

FIG. 2. (Color online) Some characteristic calculations for the three-well structure in Fig. 1(a) when it is designed with varying levels of diagonality (as characterized by f_{43}) while keeping all other parameters the same. The various symbols and terms in the plots are described in the body text.

with the CSL and BTC designs due to their very different depopulation mechanisms.

In the operating bias condition in Fig. 1(a), assuming unity injection efficiency for resonant-tunneling (RT) from $1' \rightarrow 4$, a population inversion $\Delta n_{43} \propto \tau_4[1-(1/\tau_{31}+n_2/n_3/\tau_{21})^{-1}/\tau_{4\rightarrow 3,2}]$ is established for a given current density J flowing across the structure. Approximating $n_3 \approx n_2$ (Ref. 16), a value of $(1/\tau_{31}+n_2/n_3/\tau_{21})^{-1} \approx \tau_{3,2\rightarrow 1} \approx 0.16$ ps is estimated at the operating bias, where $\tau_{3,2\rightarrow 1} \equiv (1/\tau_{31}+1/\tau_{21})^{-1}$. To quantify the role of diagonality on gain, the quantity $f_{43}\tau_4(1-\tau_{3,2\rightarrow 1}/\tau_{4\rightarrow 3,2}) \propto f_{43}\Delta n_{43}$ is computed for six different hypothetical designs where all aspects of the design are kept the same except f_{43}. Figure 2(a) shows the result of this calculation. At high temperatures, since $4 \rightarrow 3,2$ e-LO-phonon scattering is the dominant nonradiative process, $\tau_4 \approx \tau_{4\rightarrow 3,2,\mathrm{LO}} \approx \tau_{\mathrm{LO}} \exp(\hbar\omega_{\mathrm{LO}}-E_{43})/k_B T_e$, which is also plotted alongside for a particular value of $T_e=250$ K. The spatially separated wave functions in a diagonal design have a larger τ_{LO}, which increases $\tau_{4\rightarrow 3,2}$. Even though f_{43} decreases, the figure of merit $f_{43}\Delta n_{43}$ improves with diagonality. In reality, the improvement in $f_{43}\Delta n_{43}$ will be even larger than that shown in Fig. 2(a) since the injection selectivity into the level 4 also becomes better for a more diagonal design. A caveat, however, is that the radiative linewidth $\Delta\omega$ will become larger for a more diagonal design; hence the improvement in the gain $g \propto f_{43}\Delta n_{43}/\Delta\omega$ will be weaker as compared to that shown for the quantity $f_{43}\Delta n_{43}$. The quantitative dependence of $\Delta\omega$ on f_{ul} likely depends on the details of design and growth. Also note that this calculation should only be taken qualitatively since the transport through the collector barrier is not entirely coherent.[17]

A secondary advantage from increased diagonality, one that applies more to the resonant-phonon designs, is a reduction in the "parasitic" leakage current at the $1' \rightarrow 2$ alignment bias in Fig. 1(b).[12] This parasitic coupling can be characterized by the energy splitting $\Delta_{1'2}$ at the $1'-2$ anticrossing. The low-temperature threshold current density $J_{\mathrm{th,5K}}$ for these designs is believed to be limited at the low end by the current density $J_{1'2}$ at such an alignment.[16,12] $\Delta_{1'2}$ is enhanced by the spatial extent of level 3 since levels 3 and 2 are strongly coupled. For a diagonal transition, the lower level 3 is localized away from the injector barrier. Hence, $\Delta_{1'2}$ decreases with f_{43}. For a weak $1'-2$ coupling, a simplified expression $J_{1'2} \approx eN(\Delta_{1'2}/\hbar)^2\tau_{\parallel}/2$ can be written,[18] where N is the combined electron sheet density of levels $1'$ and 2 (≈QCL doping density) and $\tau_{\parallel}=[1/(2\tau_2)+1/T_2^*]^{-1}$ is the dephasing time with a phenomenological "pure" dephasing time T_2^*.[17] $J_{1'2}$ is computed using $\tau_2 \approx 0.2$ ps (calculated) and $T_2^* \approx 0.5$ ps (assumed) and is plotted along with $\Delta_{1'2}$ for different values of f_{43} in Fig. 2(b). The values of $J_{1'2} \approx 330$ A/cm^2 for $f_{43}=0.38$ and $J_{1'2} \approx 695$ A/cm^2 for $f_{43}=0.85$ (adjusted for a lower $N \approx 2.75\times 10^{10}$ A/cm^2 to correspond with that in Ref. 10) qualitatively agree with the measured values of $J_{\mathrm{th,5K}} \approx 410$ A/cm^2 for this design and $J_{\mathrm{th,5K}} \approx 700$ A/cm^2 in Ref. 10, respectively.[19]

The structure, labeled OWI222G (wafer VB0240) was grown by molecular beam epitaxy with 222 cascaded modules, with $n=5\times 10^{18}$ cm^{-3} contact layers grown above (50 nm thick) and below (100 nm thick) the 10 μm thick active region and with a 200 nm $Al_{0.55}Ga_{0.45}As$ etch-stop layer underlying the entire growth. Metal-metal waveguide ridge lasers were processed using the method outlined in Ref. 14, albeit with two variations. First, a Ta/Cu/Ti/Au layer sequence was used for the top metal to lower the waveguide losses.[10] Second, the ridges were processed by wet-etching using a 1:1:25 H_3PO_4:H_2O_2:H_2O etchant. The fabricated devices were cleaved (with back-facets left uncoated), indium soldered ridge side up on a copper mount, wire bonded, and mounted on the cold stage of a pulsed-tube (PT) cryocooler. Lasing at $\nu \sim 3.9$ THz was observed up to a heat-sink temperature of 185 K from a 120 μm × 2.04 mm ridge laser

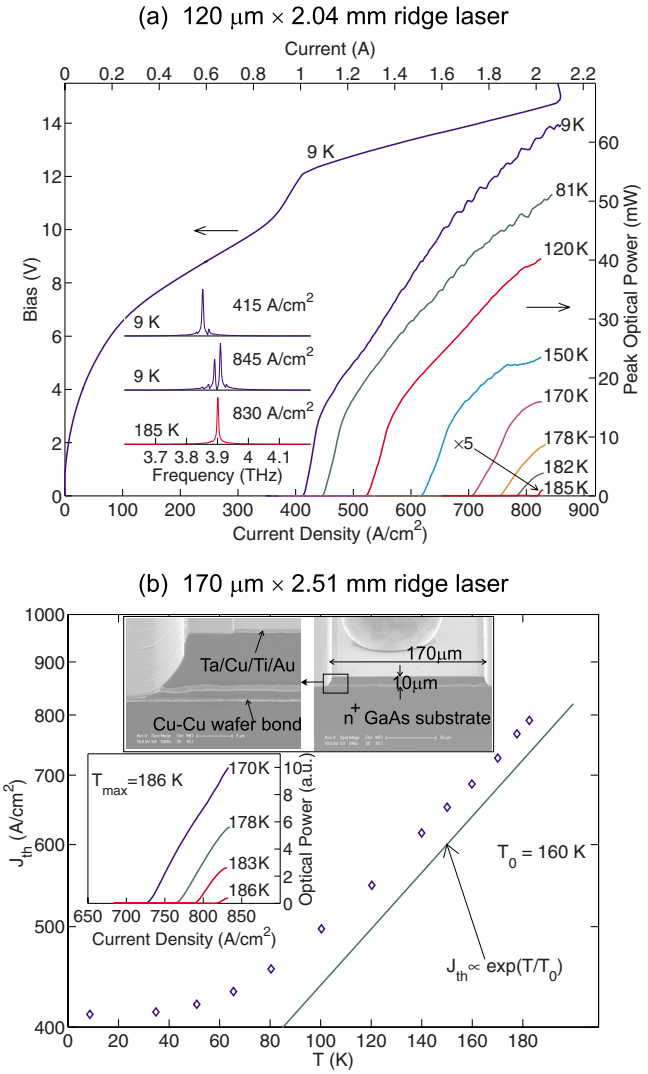

FIG. 3. (Color online) (a) Pulsed (100 ns pulses repeated at 10 kHz) light-current (*L-I*) and current-voltage (*I-V*) characteristics from a 120 μm $\times$2.04 mm ridge laser that lased up to 185 K. The inset shows some representative spectra at 9 and 185 K. The *L-I*'s and the spectra were recorded with a He-cooled Ge:Ga photodetector and a Nicolet 850 Fourier transform spectrometer. The optical power is collected from a single facet using a Winston cone. The peak power is detected with a thermopile power meter (ScienTech, model AC2500) placed adjacent to the cryostat window without any corrections. (b) Typical J_{th} vs heat-sink temperature T measurement from these lasers. A fit to the commonly used expression $J_{th} \propto \exp(T/T_0)$ is also indicated. The upper inset shows a scanning-electron microscope image of the cleaved facet of a 170 μm wide device. The lower inset shows selected high temperature *L-I*'s for the wider device of dimensions of 170 μm$\times$2.51 mm, which lased up to 186 K.

and up to 186 K from a bigger 170 μm$\times$2.51 mm device in pulsed operation. The measurement results are shown in Figs. 3(a) and 3(b), respectively. Due to wet-etching these ridges have sloped sidewalls as seen from the upper inset of Fig. 3(b). This makes the narrower ridges to have worse temperature performance since the current density is nonuniform across the modules along the vertical dimension. The *I-V* measurement is shown for the smaller device since the complete *I-V* could not be measured for the bigger device due the limitation of power supply that was used. The slope-discontinuity at $\sim$1 A in the *I-V* in Fig. 3(a) is indicative of the lasing threshold.[18] Also to be noted is the plateau region in the *I-V* at a bias of $\sim$11 V that is indicative of the $1'-2$ parasitic resonance.

The operating current densities in the range of 410 $-$830 A/cm^2 for this design are approximately a factor of two lower than that for the more vertical design in Ref. 10. This is a direct consequence of a reduced $1' \rightarrow 3,2$ leakage current in operating conditions or in other words a better injection selectivity for the $1' \rightarrow 4$ tunneling in a more diagonal design. The pulsed T_{max} of 186 K for this terahertz QCL is the highest reported so far, even though the radiative oscillator strength in this design is significantly smaller than previous designs. This confirms the presence of a larger gain at high temperatures for this active region. This design strategy is likely to yield even better performance up until the point the radiative linewidth $\Delta\omega$ becomes too broad, which offsets the advantage of a larger $f_{43}\Delta n_{43}$.

Qi Qin and Tsung-Yu Kao prepared the PT cryocooler setup used in the experiments. This work is supported by AFOSR, NASA, and NSF. Sandia is a multiprogram laboratory operated by Sandia Corporation, a Lockheed Martin Co., for the U.S. Department of Energy under Contract No. DE-AC04-94AL85000.

[1] J. Faist, F. Capasso, D. L. Sivco, C. Sirtori, A. L. Hutchinson, and A. Y. Cho, Science **264**, 553 (1994).
[2] R. Köhler, A. Tredicucci, F. Beltram, H. E. Beere, E. H. Linfield, A. G. Davies, D. A. Ritchie, R. C. Iotti, and F. Rossi, Nature (London) **417**, 156 (2002).
[3] M. Rochat, J. Faist, M. Beck, U. Oesterle, and M. Ilegems, Appl. Phys. Lett. **73**, 3724 (1998).
[4] B. S. Williams, B. Xu, Q. Hu, and M. R. Melloch, Appl. Phys. Lett. **75**, 2927 (1999).
[5] R. Köhler, A. Tredicucci, F. Beltram, H. E. Beere, E. H. Linfield, A. G. Davies, and D. A. Ritchie, Appl. Phys. Lett. **80**, 1867 (2002).
[6] A. Wade, G. Fedorov, D. Smirnov, S. Kumar, B. S. Williams, Q. Hu, and J. L. Reno, Nat. Photonics **3**, 41 (2009).
[7] G. Scalari, L. Ajili, J. Faist, H. Beere, E. Linfield, D. Ritchie, and G. Davies, Appl. Phys. Lett. **82**, 3165 (2003).
[8] S. Barbieri, J. Alton, H. E. Beere, J. Fowler, E. H. Linfield, and D. A. Ritchie, Appl. Phys. Lett. **85**, 1674 (2004).
[9] H. Luo, S. R. Laframboise, Z. R. Wasilewski, G. C. Aers, H. C. Liu, and J. C. Cao, Appl. Phys. Lett. **90**, 041112 (2007).
[10] M. A. Belkin, J. A. Fan, S. Hormoz, F. Capasso, S. Khanna, M. Lachab, A. G. Davies, and E. H. Linfield, Opt. Express **16**, 3242 (2008).
[11] B. S. Williams, H. Callebaut, S. Kumar, Q. Hu, and J. L. Reno, Appl. Phys. Lett. **82**, 1015 (2003).
[12] S. Kumar, B. S. Williams, Q. Hu, and J. L. Reno, Appl. Phys. Lett. **88**, 121123 (2006).
[13] It may be noted that for the design in Ref. 9 $f_{ul} \approx 0.85$ as opposed to its mentioned value of 0.51. The calculation of f_{ul} for these designs should be done with single-module wave functions since the injection mechanism is far from coherent (Ref. 17) and the upper radiative level u is predominantly localized in the active region.
[14] B. S. Williams, S. Kumar, Q. Hu, and J. L. Reno, Opt. Express **13**, 3331 (2005).
[15] S. Kumar, Q. Hu, and J. L. Reno (unpublished).
[16] H. Callebaut, S. Kumar, B. S. Williams, Q. Hu, and J. L. Reno, Appl. Phys. Lett. **83**, 207 (2003).
[17] H. Callebaut and Q. Hu, J. Appl. Phys. **98**, 104505 (2005).
[18] C. Sirtori, F. Capasso, J. Faist, A. L. Hutchinson, D. L. Sivco, and A. Y. Cho, IEEE J. Quantum Electron. **34**, 1722 (1998).
[19] This comparison should only be taken qualitatively since the design in Ref. 10 is different with regard to its radiative energy and the $1'-4$ coupling.